hucl-th

A study on thermodynamical properties of hot and dense hadron gas using the event generator

Nobuo Sasaki
Physics Department, Hiroshima University,
Higashi-Hiroshima 739-8526, Japan
(September 30, 2000)

Abstract

We investigate the equilibration and the equation of state of the hot hadron gas at finite baryon density using an event generator that satisfies detailed balance at temperatures and baryon densities of present interests ($80 < T < 170$ MeV, $0.157 < n_B < 0.315\text{fm}^{-3}$) . Molecular-dynamic-simulations are performed to the system of hadrons in the box with periodic boundary conditions. Starting from an initial condition composed of nucleons with uniform momentum distribution, the evolution takes place through interactions, productions and absorptions. The system approaches to a stationary state of baryons, mesons and their resonances. The system is characterized by an exponent in the energy distribution irrespective of the particle species, i.e., temperature. After the equilibration, thermodynamical quantities such as energy density, particle density, entropy and pressure are calculated. Obtained equation of state shows a remarkable deviation from the mixed free gas of mesons and baryons above $T \sim m_\pi$. Large values of entropy per baryon is also seen. There, enhancement of excitation of heavy baryon resonances and meson productions occurs simultaneously and rising of the temperature becomes moderate. Pressures show linear dependence on energy density, and sound velocity is smaller than $\sqrt{\frac{1}{3}}$.

25.75.-q, 24.10.Lx, 05.70.-a

I. INTRODUCTION

From a viewpoint of microscopic dynamics, hot and dense hadron gas has some unique properties. For example, the coexistence of relativistic particles and non-relativistic heavy particles, productions and absorptions of particles/anti-particles, large degrees of freedom for species of resonances are quite different from nature of classical molecular dynamic systems. Properties of such hadron gas on-equilibrium and off-equilibrium are nontrivial and an interesting target of theoretical challenge. Among them, equation of state (EOS) and transport coefficients of hot and dense hadron gas are attractive topics both in high-energy nuclear physics and cosmology. In ultra-relativistic heavy-ion experiments at CERN and BNL, although many efforts are devoted to the search for Quark-Gluon Plasma (QGP) [1], physics of a hadron gas dominates the system. Thus, studying the EOS and transport coefficients of a hadron gas is necessary for the interpretation of experimental results such as the analysis of flow [14]. In cosmology, inhomogeneous nucleosynthesis at early universe is an attractive possibility for the origin of the matter and baryon diffusion constant is a key quantity in this scenario [2].

In spite of their great importance, the EOS and transport coefficients of hot and dense hadron gas are still poorly known, mainly because of a non-perturbative character of the strong interaction. Lattice QCD is a powerful tool for the non-perturbative QCD. Actually, lots of calculations about EOS of hot quark-gluon plasma phase have been performed [3] [4] [5]. However, investigation in hadron phase is still difficult and no useful result has been obtained yet. Inclusion of chemical potential is more difficult for lattice QCD in spite of several approaches [6] [7]. Moreover, the study of transport coefficients is not so advanced, although those of hot gluonic matter have been evaluated recently [8].

In phenomenology, many thermodynamical models are proposed. Hagedorn has proposed bootstrap model in old days and existence of limiting temperature has been claimed [9]. On the contrary, hot and dilute hadron gas is often regarded as an ideal gas of massless pion and massive baryons. Since pion is Nambu-Goldstone mode that is excited predominantly, this picture seems a reasonable starting point. But residual interaction is not negligible. This simple picture is partly corrected by including a finite volume of hadrons, i.e., excluded volume effect [10] such as van der Waals equation. However, there is no confirmation whether such approximation is proper or not. Although the excluded volume imitates the effect of repulsion between hadrons, microscopic interactions of a hot and/or dense hadron gas is much more complicated and role of them is not obvious. Thus, we attempted to study the thermodynamical nature of a hadron gas using a microscopic model, which includes interactions among hadrons [11].

In this paper, we perform a molecular-dynamic simulations to the system of hadron gas using an event generator which describes interactions among hadrons. Set of statistical ensembles are produced by an event generator URASiMA (Ultra-Relativistic AA collision Simulator based on Multiple scattering Algorithm) [15] [16] [17]. For those ensembles, thermodynamical quantities are evaluated and EOS of a hadron gas is obtained. Transport coefficients are also obtainable, but we leave the study of them to another paper [12].

In our previous work, we have made a pilot study of equation of state of a hot and dense hadron gas by the generator [11]. In the work, approximate saturation of temperature like the Hagedorn's limiting temperature is seen. Recently, Belkacem et al., performed a

similar calculation using a different event generator UrQMD [18]. They also have reported the saturation of the temperature [19]. Although those works gave valuable hints to the nature of the hadron gas, some results are doubtful because the detailed balance of the processes is broken. Both models don't include multi-body absorptions that are reverse processes of multi-particle production. For energetic hadrons in a closed system, we need both processes to ensure detailed balance. If the detailed balance is broken, the reversibility of the equilibrated system is realized no longer.

Although it is interesting and important to formulate these multi-body absorption processes exactly in the simulation, straightforward implementation of them is very difficult and not practical. In this paper, we avoid solving this complicated problem and take a practical way. We improve URASiMA to conserve the detailed balance at temperatures of present interest by adopting the idea, which we see later in the next section.

In section II, we describe the method of our simulation. In section **??**, we introduce URASiMA and state the improvement to recover detailed balance effectively. In section IV, we show the equation of state of the hadron gas, and compare them with that of the free gas model. Section V is a summary of this paper.

II. METHOD OF SIMULATION

A. Geometry and boundary condition

In this work, we concentrate on the thermodynamical nature of hadronic system. For this purpose, we put the system in a cubic box and impose the periodic boundary condition for motion of particles, i.e., if a particle goes out from the box, another one with the same momentum comes in from the other side. We show the boundary condition pictorially in fig.1, where the box locating in the center is that of our interest, thus we call it the real box and the others are replicas. When we survey would-be collision points between particles in the real box, we also have to survey those between a particle in the real box and another particle in a replica.

The obtained result should be insensitive to the box size. Later we will examine finite size effect in the present treatment. In any case, it is certain that a side of the box l should be longer than the mean free path of hadrons,

$$l \gg \frac{1}{\rho \cdot \sigma}, \tag{1}$$

where ρ is a particle density of the system, and σ denotes a total cross section.

B. Generation of statistical ensemble

The total energy density ε and the baryon number density n_B in the box are fixed as input parameters. These quantities are conserved throughout the simulation. Though initial particles are only nucleons, many mesons are produced through interactions. Initial distributions of nucleons are given by uniform random distributions in a phase space. Momenta of particles are adjusted to satisfy the total energy conservation, $\sum_{i=1}^{N} \sqrt{m_i^2 + p_i^2} = \varepsilon \cdot V$ in

C.M. system of particles, i.e., $\sum_{i=1}^{N} \vec{p_i} = 0$. After such initialization, the time evolution is performed by URASiMA.

In order to confirm onset of the stationary state, we monitor particle densities or collision frequencies. We also check energy distributions at regular time intervals. As time goes on, system becomes stationary. A fundamental question is that energy distributions should approach to Boltzmann distribution

$$\frac{dN}{d^3\vec{p}} = \frac{dN}{4\pi E p dE} = C \exp(-\beta E), \tag{2}$$

where β is a slope parameter of the distribution. When the system is in thermal equilibrium, slope parameters of all particles should become common value, i.e., inverse of temperature. To see this, we analyze the time evolution of inverse slopes β^{-1} for various particles.

C. Evaluation of thermodynamical quantities

Running URASiMA many times with the same input parameter and taking the stationary configuration later than the establishment of thermal and chemical equilibrium, we obtain statistical ensemble with fixed temperature and fixed baryon number density.

Using the ensemble, thermodynamical quantities such as energy density, particle density, pressure, and so on, are obtained as a function of temperature and baryon number density. In this way, we study equation of state of mixed hadron gas.

III. EVENT GENERATOR URASIMA

A. Overview

URASiMA is originally designed to perform the simulation of ultra-relativistic heavy-ion experiments. In this work, we make use of URASiMA as the generator of hadron-hadron collisions. Several characteristics of URASiMA is shown below.

Fundamental processes are hadronic 2-body collisions between hadrons. Elastic as well as inelastic collisions are included. As for the latter, both quasi-two body scattering and multi-production are counted. We use available experimental data as possible as we can [20].

In the system, collisions are generated when impact parameter between particles becomes smaller than their interaction range determined by relevant total cross-sections. In appendix A, we describe our method to search the would-be collision points. Particle species and quasi-two body collisions are summarized in III B.

In addition to the collisions, strong decays of hadrons are taken into account. Nucleon resonances and rho mesons are decaying particles in this model.

An important aspect of the generator is that detailed balance is maintained effectively. Reverse processes of quasi-two-body collisions and decays are properly incorporated as described in III B. They are not important in cases of high energy hadron/nuclear collisions but are essentially important in the studies of the thermo-equilibrium systems.

In order to demonstrate describability of the model, we compare the model with the high energy nuclear collisions at BNL/AGS in III D.

B. Particle species and quasi-two-body processes

As we have already mentioned, quasi-elastic collisions are a main contribution to particle productions at energies of present interest. Following processes produce baryon resonances,

$$NN \to NR, \tag{3a}$$

$$NN \to \Delta_{1232}\Delta_{1232}, \tag{3b}$$

where N and R denote nucleons and baryon resonances, respectively. URASiMA includes Δ's and N^*'s whose masses are up to 2 GeV (See table I). For the calculation of cross sections about these processes, we follow the work of S. Teis, et al [21] [22].

We take account of decays of resonances. Accepted decay modes are as follows,

$$R \to N\pi, \tag{4a}$$

$$R \to R'\pi, \tag{4b}$$

$$R \to Nr, \tag{4c}$$

where r denotes meson resonances, which can decay into 2π,

$$r \to \pi\pi. \tag{5}$$

At low energies, 1π and 2π production processes are dominated by quasi-elastic resonance productions (eq.(3)) and their successive decays (eq.(4), eq.(5)). Actually, we can reproduce the inelastic cross section of NN collision up to $\sqrt{s} = 3$ GeV. However, if $\sqrt{s}$ is above 3 GeV, contributions of nπ ($n \geq 3$) productions are not negligible.

For the treatment of 1π and 2π absorption processes, following resonance formations are included.

$$\pi\pi \to r, \tag{6a}$$

$$N\pi \to R, \tag{6b}$$

$$Nr \to R, \tag{6c}$$

$$R\pi \to R'. \tag{6d}$$

They are inverse processes of decays. Cross sections of eq.(6) are calculated from Breit-Wigner formula. Moreover, URASiMA contains resonance absorption processes,

$$NR \to NN, \tag{7a}$$

$$\Delta_{1232}\Delta_{1232} \to NN. \tag{7b}$$

By using reciprocity of S matrix, relation between the production cross section and the absorption cross section is given by

$$\sigma_{N''R\to NN'} = \frac{2}{g_R}\frac{1}{1+\delta_{NN'}}\frac{p_f^2}{p_i^2}\sigma_{NN'\to N''R}, \tag{8}$$

where $\delta_{NN'}$ is Kronecker's δ which is equal to 1 when final state nucleons cannot be distinguished. The relation (8) is valid for particles with definite mass. Thus we should take into account the width of resonance mass. After some calculations, the absorption cross section is written as

$$\sigma_{N''R\to NN'} = \frac{2}{g_R}\frac{m_R p_f^2}{1+\delta_{NN'}}\frac{\sigma_{NN'\to N''R}}{p_i\int_{m_\pi+m_N}^{\sqrt{s}-m_N}\frac{dm_R'}{2\pi}m_R'\rho_R(m_R')p_i'}. \tag{9}$$

where $\rho_R(m_R')$ is the mass distribution function which is given by Breit-Wigner distribution [23] [24].

Including processes from eq.(3) to eq.(7), the detailed balance between 1π, 2π productions and 1π, 2π absorptions is realized.

C. Multi-particle productions

In high energy hadron-hadron collisions, n-particle ($n \geq 3$) productions may occur. In our model, such multi-particle productions are treated as direct processes. In a stage where energetic particles are dominated, such processes are very important. In the present treatment, initial states include energetic nucleons and multi-particle production takes place in the beginning stage. In the later stage, they are not frequent and their effect is negligibly small.

In URASiMA, multi-particle production process is realized based on Multi-Chain Model where exchange of hadronic chain causes direct emission of multipions.

Figure 2 shows a diagram of $N+N$ inelastic collisions. In this figure, leading nucleons exchange a chain, which produces secondary particles. Such a multi-particle production is specified by following parameters. Probability distribution of light-like longitudinal momentum fraction x_N, which is carried by nucleons after collisions, is given by

$$P(x_N) = \alpha \cdot x_N^{\alpha-1}. \tag{10}$$

The average energy which is carried by leading nucleons is $\alpha/(\alpha+1)$ times the initial energy. The remainder which is in an average equal to $1/(\alpha+1)$ is consumed by the production of secondary particles.

In the C.M. frame of produced particles, the longitudinal momentum of the secondary particle is determined according to the following distribution

$$\frac{dN}{dy} \propto (1-\frac{2m_T\cosh y}{\sqrt{\hat{s}}})^\beta, \tag{11}$$

where m_T is the transverse mass of a secondary particle, y is the rapidity, and $\sqrt{\hat{s}}$ is the energy that is deposited in the blob of the diagram.

Transverse momentum distributions of leading and secondary particles are given by gamma distributions,

$$\frac{dN_j}{dp_T} \propto p_T e^{-B_j \cdot p_T} \qquad (j = \text{nucleon}, \ \ \pi, \ \ etc.), \tag{12}$$

where p_T denotes the transverse momentum and B_j is the slope parameter and it is another parameter of the model.

Secondary particles propagate freely without any interaction during the formation time τ after the emission,

$$\tau = \gamma \cdot \tau_0 = \frac{E}{m} \cdot \tau_0, \tag{13}$$

where the proper formation time τ_0 is also one of parameters of URASiMA.

D. Comparisons with data of Nucleus-nucleus collisions at high energies

In order to examine descriptive power of the generator, comparisons with the data of high-energy nuclear collision are made. In this case, the generator is applied for the initial set of energetic nucleons forming nuclei in free space. The parameters, α and β , are already tuned to reproduce the data of hadron-hadron collisions.

Results of our simulations are compared with experimental data of E802 collaboration for S + Al central collision at 14.6 GeV/nucleon [25]. Fig.3 shows rapidity distributions for proton (left) and π^+ (right), where squares denote results of our simulation, and filled circles are experimental results. Similarly, fig.4 shows the rapidity dependence of inverse slopes of transverse momentum distributions for proton (left) and π^+ (right).

Through the comparisons, we find that URASiMA well reproduces global features of experimental data.

IV. RESULTS

A. Input parameters

Input parameters are given in table II. Here $n_B = 0.156$ [fm^{-3}] corresponds to the baryon density of the normal nuclear matter. Thus, the baryon number density of our study is $1 \sim 2$ times larger than that of the normal nuclear matter. The total isospin of the system is set to zero, i.e., the total number of protons is equal to that of neutrons at the start.

B. Equilibration and temperature of the system

At first, we check the finite size effect in the present result. Figure 5.(a),(b) are time evolutions of particle densities at $V = 64.0$ fm^3. Similarly, fig.5.(c),(d) show same quantities

at $V = 128.0$ fm^3. The volume dependence of particle densities is not observed. Fig.10 shows the temperature at various initial conditions. Results at $V = 64.0$fm^3 and $V = 128.0$fm^3 are compared. The volume dependence of temperature is not observed. From these results, we conclude that the volume $V = 64.0$fm^3 is enough large and our simulations properly reproduce an infinite system.

Figure 5 shows that the system comes to the stationary state as time passes. Such saturations of particle densities indicate an achievement of chemical equilibrium. However, studying the detailed balance of individual reaction processes is necessary for the conclusive evidence.

In fig.6, we present time evolutions of collision frequencies $[(\mathrm{fm/c})^{-1}]$ for all kinds of reaction processes. From this figure, the collision frequency of the multi production is less than 10^{-3} $[(\mathrm{fm/c})^{-1}]$ in the later stage, and the time scale is much longer than other processes. Violation of reciprocity is relevant only for such long development. As shown in fig.7, detailed balance actually holds in the time scale of several hundred fm/c. Thus we conclude that the chemical equilibrium of the system is almost established.

Fig.8 shows energy distributions of $N_{938}, \Delta_{1232}, \pi$ and ρ_{770} at $t = 5,\ 10,\ 50$ fm/c. We plot results as a function of kinetic energy $K = E - m$, because bases of horizontal axis for all particle species agree with. As time passes, energy distributions approach to Boltzmann distributions, see eq.(2). Moreover, slopes β of energy distributions converge to the same value. These results indicate that the achievement of thermal equilibrium. Fig.9.(a) shows the time evolution of β^{-1}s that are calculated from the fitting of energy distributions by Boltzmann distribution, where dotted lines correspond to the time evolution of β_π^{-1}, i.e., an inverse slope of π. The statistical error of β_π^{-1} is comparatively small, thus β_π^{-1} is compared to inverse slopes of other particles.

To confirm that the thermal equilibrium establishes, following quantities are defined at time t,

$$\Delta\beta_j^{-1}(t) = \beta_j^{-1}(t) - \beta_\pi^{-1}(t), \tag{14}$$

where j corresponds to N_{938}, Δ_{1232} and ρ_{770}. Fig.9.(b) shows the time evolution of $\Delta\beta_j^{-1}$. In this figure, the time when values of $\Delta\beta_j^{-1}$ become zero in the accuracy of statistics is about 150 fm/c. Consequently, we conclude that the thermal equilibrium establishes at $t \sim 150$ fm/c, i.e., inverse slope parameters of energy distribution of all particles become the same value at this time. Thus we call this value as the temperature of the system. We define the temperature as follows,

$$T(n_B, \varepsilon) = \frac{\sum_j \beta_j^{-1}/\sigma_j^2}{\sum_j 1/\sigma_j^2} \qquad j = N_{938}, \Delta_{1232}, \pi \ \text{ and } \ \rho_{770}, \tag{15}$$

where β_j are calculated from energy distributions that are averaged over time after $t =$ 200fm/c, and σ_j denote errors of β_j.

Here we briefly refer to the time scale of the relaxation of the system. Fig.5 shows that the number density $n(t)$ seems to be relaxed exponentially,

$$\begin{aligned} n(t) &= (n_B - n(\infty)) \cdot e^{-\frac{t}{\tau}} + n(\infty) \qquad N, \\ n(t) &= n(\infty) \cdot (1 - e^{-\frac{t}{\tau}}) \qquad \Delta,\ \pi,\ \rho. \end{aligned} \tag{16}$$

Based on this fact, we can easily estimate the relaxation time τ of particle densities that approach to the chemical equilibrium. We show results on nucleon, pion and ρ densities in table III. As for nucleon and pion densities, the value of τ is $7 \sim 20$ fm/c, and is dependent on energy density. On the other hand, we have remarkably larger value for ρ.

Song and Koch calculated chemical relaxation time of pions in hot hadron gas using the effective chiral Lagrangian [26]. They estimate a chemical relaxation time of 10 fm/c for π at $T \sim 150$ MeV. Their results are consistent with present results. Moreover, table III shows that some different time scales exist, and one of them is remarkably long, although these values may be dependent on the initial condition of the simulation. Namely, our results indicate the possibility that a system has a long relaxation time in a certain case. The more systematic study of the relaxation time will be in our future plan.

C. Study of equation of state

Fig.11$\sim$13 shows the relation between the temperature and thermodynamical quantities such as the energy density, the number density and the pressure. In these figures, all lines correspond to the equation of state of the relativistic Fermi-Dirac or Bose-Einstein gas with a finite width of mass, i.e.,

$$\varepsilon(T,\mu) = \sum_h d_h \int\int \frac{dmd^3p}{(2\pi)^3} \frac{\rho_R(m)E}{e^{\frac{E-\mu}{T}} \pm 1}, \tag{17a}$$

$$n(T,\mu) = \sum_h d_h \int\int \frac{dmd^3p}{(2\pi)^3} \frac{\rho_R(m)}{e^{\frac{E-\mu}{T}} \pm 1}, \tag{17b}$$

$$P(T,\mu) = \sum_h d_h \int\int \frac{dmd^3p}{(2\pi)^3} \rho_R(m) \ln(1 \pm e^{\frac{-(E-\mu)}{T}}), \tag{17c}$$

where d_h denotes a degeneracy factor and $\rho_R(m)$ is the mass spectral function which is given by Breit-Wigner distribution for resonances. In this model, the baryon chemical potential μ_B is adjusted to reproduce the total baryon number density whereas the meson chemical potential μ_m is fixed to zero.

In eq.(17), anti-baryons are neglected because our event generator does not include anti-baryons. However, their contributions to values of the baryon chemical potential are almost negligible if the temperature is below 170 MeV, since a ratio of an anti-baryon number to a baryon number is given by $e^{-\frac{2\mu_B}{T}}$. At the smallest value of the chemical potential $\mu_B \sim 250$MeV ($n_B = 0.157$ fm^{-3}, $T = 170$MeV), the ratio is about 5 % at most.

Fig.11$\sim$13.(a),(b) are equation of state of baryon. In these figures, it is difficult to see the difference between our results and the calculation of the free gas model. This behavior is inevitable because the baryon number conservation constrains the sum of number densities for N and Δ. So a close look at fractions of baryon resonances is in order.

Fig.14 shows particle ratios of N_{938}, Δ_{1232} and other heavy resonances N^*, Δ. At comparatively low temperature ($T = 125$ MeV), the difference between our results and free gas calculations is small. On the other hand, at high temperature ($T > 150$ MeV), ratios of light

baryons (N_{938} and Δ_{1232}) are suppressed, and those of heavy resonances are conversely enhanced. Thus we find that the influence of interactions becomes visible above $T \sim m_\pi$. Such an enhancement of heavy baryons grows as the increase of the temperature. The maximum value of the enhancement is about $12 \sim 15\%$ at $T \sim 170$ MeV.

Fig.11$\sim$13.(c),(d) show EOS of mesons. Similarly, the deviation from the free gas model is observed above $T \sim m_\pi$. Above this temperature, meson productions are excited and the rising of the temperature becomes moderate. However, the limiting temperature is no more observed [11] [19], thus our results cannot be explained by the simple Hagedorn gas picture. Effects of interactions are more complicated.

Moreover, our results indicate that equation of state of baryons and mesons are closely related each other through meson-baryon interactions such as $\pi N \rightarrow R$ and their inverse processes. Actually, the enhancement of heavy baryon resonances causes the increase of abundances of mesons, and vice versa. It is understood as follows. Heavy resonances easily produce 2π, thus the enhancement of heavy baryon resonances promotes meson productions. Consequently, interactions between meson and baryon are very important to discuss the property of the mixed hadron gas.

Fig.15 is the entropy per baryon versus the temperature. In our calculation, the definition of the entropy is given by

$$S = -Tr < \rho(\boldsymbol{x}, \boldsymbol{p}) > \ln(< \rho(\boldsymbol{x}, \boldsymbol{p}) >), \tag{18}$$

where $< \rho(\boldsymbol{x}, \boldsymbol{p}) >$ is the ensemble average of the density operator. The density operator $\rho(\boldsymbol{x}, \boldsymbol{p})$ is defined on the the phase space $\Delta^3 x \cdot \Delta^3 p$, whose volume is equal to $(\hbar c)^3 \mathrm{fm}^3 \cdot (\mathrm{GeV/c})^3$. If a particle exists in one of volume elements, the value of $\rho(\boldsymbol{x}, \boldsymbol{p}) = 1$. Here lines are corresponding to free gas calculations. Fig.15 shows that the hadron gas has a larger value of S/N_B than that of the free gas model for $T > m_\pi$, because a greater part of the energy of the system is consumed by particle (entropy) productions. Moreover, our results show a clear dependence on the baryon density. Thus the frequently used approximation that S/N_B is insensitive to n_B is no more valid. Consequently, our result indicates that the free gas model is a poor description for this quantity above $T > m_\pi$. So it should be careful to use a free gas model to interpret the ultra-relativistic heavy ion experiments, even if some corrections like the excluded volume effect are considered [27] [28] [29].

Furthermore, some models seem insufficient to count dynamical degree of freedom per baryon. For example, EOS based on $\sigma - \omega$ model [30] predicts $S/N_B \sim 5$ (see ref. [33]) irrespective of temperature while our result shows $S/N_B \sim 18.6 \pm 0.2$ at $T = 150$ MeV and 29.2 ± 0.1 at $T = 170$ MeV for the normal nuclear matter density. Baryon resonances such as Δ and N^* are important and they should be included in the calculations.

Finally we see relations between energy densities and pressures. We measure the pressure as follows,

$$P = \frac{1}{3V} \sum_{i=1}^{\text{all particles}} \frac{p_{ij} p_i^j}{E_i} \qquad (j = x, y, z). \tag{19}$$

From fig.16.(a), we find that our results and free gas calculations show almost a linear dependence of the pressure on the energy density within the range of present study. It indicates the constant value of the sound velocity $v_S \equiv \sqrt{\frac{\partial P}{\partial \varepsilon}}$. Our results can be fitted by the following function,

$$P = v_s^2 \cdot (\varepsilon - \varepsilon_0). \tag{20}$$

Values of the parameters at three different baryon number densities are shown in table IV. Obtained values of the sound velocity are smaller than those of the free gas. It is noted that this quantity has been calculated on the quenched lattice [5].

To clarify the situation further, we examine partial pressures. As we have shown in fig.11∼13.(a),(b), pressures and energy densities of baryons versus the temperature are not so deviated from the free gas. As for the partial pressure of mesons, non-trivial feature is seen. In fig.16.(b), partial pressures of mesons are plotted versus partial energy densities of them. It is interesting that pions behave like free gas for this quantity. On the other hand, the slope of ρ meson is smaller than that of the free gas. In fig.11.(c),(d), we find that π and ρ have almost the same energy density at high temperature. Thus, it is natural that the reduction of the sound velocity is caused by ρ meson. This result indicates the important role of ρ meson and its interactions for the thermodynamical property of hadron gas.

V. SUMMARY

In this paper, we study the equilibration and the equation of state of the hot ($80 < T < 170$ MeV) hadron gas that has the finite baryon density ($0.157 < n_B < 0.315$ fm^{-3}) using the event generator URASiMA, which conserves the detailed balance at temperatures of present interests. We perform molecular dynamic calculation to the system of hadrons in the box with periodic boundary conditions.

Collision frequencies and number densities show the saturation as the time evolution proceeds. These results indicate the chemical equilibration of the system. We also study the thermal equilibration of the system from the time evolution of inverse slopes of energy distributions. To confirm that the thermal equilibrium establishes, it is demonstrated that slope parameters of N_{938},Δ_{1232}, π and ρ_{770} become identical at $t \sim 150$ fm/c. Thus the temperature of the system can be defined after this time.

After the equilibration, thermodynamical quantities are estimated and the equation of state is studied. Energy densities, number densities, pressures and entropies per baryon are plotted versus the temperature. Deviations from the free gas model are manifestly observed above $T \sim m_\pi$. Above this temperature, excitation of heavy baryon resonances are enhanced, and meson productions are frequent. Those effects suppress rising of the temperature. A simple phenomenological picture such as Hagedorn gas model, cannot explain those behavior. In order to understand this feature, meson-baryon interactions are essentially important.

We find large values of entropy per baryon. It strongly depends on the baryon density above $T \sim m_\pi$.

Pressures show linear dependences on energy densities within the range of present study, thus constant values of sound velocity are estimated. Although the free gas model also gives constant sound velocities, whose values are larger than those of our results. Such a behavior is studied in detail by looking at relations between partial pressures of mesons and partial energy densities of them.

Acknowledgment

We would like to thank O. Miyamura, S. Muroya, and C. Nonaka for helpful discussions. Calculation has been done at Institute for Nonlinear Sciences and Applied Mathematics, Hiroshima University.

APPENDIX: THE SEARCH OF WOULD-BE COLLISION POINTS

Consider an n-particle system. If a particle i collides with one of other particles at a space-time point $x^\mu_{0\,i} = (t_{0\,i}, \boldsymbol{x}_{0\,i})$, the orbit of this particle after the collision is given by the straight line

$$x^\mu_i = (t_i, \boldsymbol{x}_i) = \frac{p^\mu_i}{m_i}\xi_i + x^\mu_{0\,i}, \tag{A1}$$

where $p^\mu_i = (E_i, \boldsymbol{p}_i)$ and m_i are the momentum and the mass of the particle after the collision. Here we use the proper time ξ_i which is defined as

$$\xi_i \equiv \frac{m_i}{E_i}(t_i - t_{0\,i}). \tag{A2}$$

Equation (A1) is available until the next binary collision changes p^μ_i and m_i. Thus the possibility of new collisions should be searched.

We adopt hard sphere approximation for binary collisions, that is, the collision occurs whenever the following condition is satisfied

$$\pi \boldsymbol{b^*}^{\,\boldsymbol{2}} < \sigma, \tag{A3}$$

where $|\boldsymbol{b^*}|$ denotes the impact parameter in the CM frame of two particles, and σ denotes the total cross section. It is useful to express the collision condition (A3) covariant way.

For this purpose, we consider the CM frame of two particles 1 and 2. See fig.17. When two particles are at the closest point, the impact parameter $\boldsymbol{b}^* \equiv \boldsymbol{x}^*_1(t^*_1) - \boldsymbol{x}^*_2(t^*_2)$ and the time t^*_c are defined as

$$\begin{aligned} (\boldsymbol{x}^*_1(t^*_1) - \boldsymbol{x}^*_2(t^*_2)) \cdot \boldsymbol{p}^*_j = 0 \qquad (j = 1, 2), \\ t^*_1 = t^*_2 \equiv t^*_c, \end{aligned} \tag{A4}$$

where t^*_c denotes the time when collision may occur. Here we define the total momentum $Q^{\mu*}$ and the difference of momenta $K^{\mu*}$,

$$\begin{aligned} Q^{\mu*} &\equiv p^{\mu*}_1 + p^{\mu*}_2 = (E^*_1 + E^*_2, 0), \\ K^{\mu*} &\equiv p^{\mu*}_1 - p^{\mu*}_2 = (E^*_1 - E^*_2, \boldsymbol{p}^*_1 - \boldsymbol{p}^*_2). \end{aligned} \tag{A5}$$

Using $Q^{\mu*}$ and $K^{\mu*}$, eq.(A4) is rewritten as

$$\begin{aligned} (\boldsymbol{x}^*_1(t^*_1) - \boldsymbol{x}^*_2(t^*_2)) \cdot \boldsymbol{K}^* = 0, \\ (t^*_1 - t^*_2) Q^{0*} = 0. \end{aligned} \tag{A6}$$

The invariant expressions of eq.(A6) are easily obtained as follows

$$(x_1 - x_2) \cdot Q = 0,$$
$$(x_1 - x_2) \cdot K = 0. \tag{A7}$$

Replacing x_1, x_2 in eq.(A7) by eq.(A1), we find simultaneous equations for proper time ξ_1 and ξ_2,

$$\frac{p_1 \cdot Q}{m_1}\xi_1 - \frac{p_2 \cdot Q}{m_2}\xi_2 + X_0 \cdot Q = 0,$$
$$\frac{p_1 \cdot K}{m_1}\xi_1 - \frac{p_2 \cdot K}{m_2}\xi_2 + X_0 \cdot K = 0, \tag{A8}$$

where $X_0^\mu = x_{0\,1}^\mu - x_{0\,2}^\mu$. Solutions of these equations are as follows,

$$\begin{pmatrix} \xi_1 \\ \xi_2 \end{pmatrix} = \frac{-1}{J} \begin{pmatrix} -\frac{p_2 \cdot K}{m_2} & \frac{p_2 \cdot Q}{m_2} \\ -\frac{p_1 \cdot K}{m_1} & \frac{p_1 \cdot Q}{m_1} \end{pmatrix} \begin{pmatrix} X_0 \cdot Q \\ X_0 \cdot K \end{pmatrix}, \tag{A9}$$

where J is defined as

$$J \equiv -\frac{(p_1 \cdot Q)(p_2 \cdot K) - (p_1 \cdot K)(p_2 \cdot Q)}{m_1 m_2}$$
$$= -2\frac{(p_1 \cdot p_2)^2 - (m_1 m_2)^2}{m_1 m_2}. \tag{A10}$$

Using eq.(A1) and eq.(A9), the invariant expression of the impact parameter is given by

$$b^2 \equiv (x_1 - x_2)^2$$
$$= X_0^2 - \frac{(X_0 \cdot Q)^2}{Q^2} - \frac{[(X_0 \cdot K) - \frac{(K \cdot Q)(X_0 \cdot Q)}{Q^2}]^2}{(K - \frac{(K \cdot Q)}{Q^2}Q)^2}. \tag{A11}$$

This expression allows us to specify the collision point by momenta and space-time coordinates at the starting points. In the simulation, all candidates of collisions are searched by eq.(A11) and the earliest collision in the rest frame of the box is generated.

REFERENCES

[1] For example, see the proceedings of Quark Matter '99, Nucl. Phys. **A661**, 3c (1999).
[2] T. Kajino, Phys. Rev. Lett. **66, 125 (1991).**
[3] By F. Karsch, E. Laermann and A. Peikert, Phys. Lett. B478,447 (2000).
[4] M. Okamoto *et al.*, CP-PACS Collaboration, Phys. Rev. D60, 4510 (1999).
[5] G. Boyd, J. Engels, F. Karsch, E. Laermann, C. Legeland, M. Lutgemeier, B. Petersson, Nucl. Phys. B469, 419 1996.
[6] I. M. Barbour *et al.*, UKQCD Collaboration, Nucl. Phys. A642, 251 (1998).
[7] O. Kaczmarek, J. Engels, F. Karsch, and E. Laermann, in proceedings of 17th International Symposium on Lattice Field Theory (LATTICE 99), hep-lat/9908046.
[8] S. Sakai, A. Nakamura, and T. Saito, Nucl. Phys. A638, 535c (1997).
[9] R. Hagedorn, cern-th-7190-94 (1994).
[10] M. I. Gorenstein, A. P. Kostyuk, and Ya. D. Krivenko, J. Phys. G25, 75 (1999).
[11] N. Sasaki, and O. Miyamura, Prog. Theor. Phys. Suppl. 129, 39 (1997).
[12] N. Sasaki, O. Miyamura, S. Muroya, and C. Nonaka, Phys. Rev. C62, 1901 (2000).
[13] N. Sasaki, O. Miyamura, S. Muroya, and C. Nonaka, in preparation.
[14] C. Nonaka, E. Honda, and S. Muroya, in preparation.
[15] K. Kinoshita, A. Minaka, and H. Sumiyoshi, Prog. Theor. Phys. 61, 165 (1979).
[16] T. Kanki, K. Kinoshita, H. Sumiyoshi, and F. Takagi, Prog. Theor. Phys. Suppl. 97A (1988); T. Kanki, K. Kinoshita, H. Sumiyoshi, and F. Takagi, Prog. Theor. Phys. Suppl. 97B (1989).
[17] S. Daté, K. Kumagai, O. Miyamura, H. Sumiyoshi, and X. Z. Zhang, J. Phys. Soc. Jpn. 64, 766 (1995).
[18] S. A. Bass *et al.*, Prog. Part. Nucl. Phys. 41, 225 (1998).
[19] M. Belkacem *et al.*, Phys. Rev. C58, 1727 (1998).
[20] Landolt-Börnstein 12, Total Cross-Sections for Reactions of High Energy Particles.
[21] S. Teis *et al.*, Z. Phys. A356, 421 (1997).
[22] V. Dmitrev *et al.*, Nucl. Phys. A459, 503 (1986).
[23] Gy. Wolf *et al.*, Nucl. Phys. A545, 139 (1992).
[24] Bao-An Li, Nucl. Phys. A552, 605 (1993).
[25] T. Abbott *et al.*, E-802 Collaboration, Phys. Rev. C50, 1024 (1994).
[26] C. Song and V. Koch, Phys. Rev. C55, 3026 (1997).
[27] P. Braun-Munzinger, J. Stachel, J. P. Wessels, and N. Xu, Phys. Lett. B344, 43 (1995).
[28] P. Braun-Munzinger, J. Stachel, J. P. Wessels, and N. Xu, Phys. Lett. B365, 1 (1996).
[29] P. Braun-Munzinger, I. Heppe, and J. Stachel, Phys. Lett. B465, 15 (1999).
[30] D. H. Rischke, Y. Pürsün, and J. A. Maruhn, Nucl. Phys. A595, 383 (1995).
[31] C. P. Singh, B. K. Patra, and K. K. Singh, Phys. Lett. B387, 680 (1996).
[32] H. Kouno, and F. Takagi, Z. Phys. C45, 43 (1989).

[33] M. Reiter, A. Dumitru, J. Brachmann, J. A. Maruhn, H. Stöcker, and W. Greiner, Nucl. Phys. A643, 99 (1998).

TABLES

TABLE I. Baryons, mesons and their resonances included into the URASiMA.

N	N_{938}	N_{1440}	N_{1520}	N_{1535}	N_{1650}	N_{1675}	N_{1680}	N_{1720}
Δ	Δ_{1232}	Δ_{1600}	Δ_{1620}	Δ_{1700}	Δ_{1905}	Δ_{1910}	Δ_{1950}	
meson	π	σ_{800}	ρ_{770}					

TABLE II. Input parameters. Here V denotes a volume of the box, n_B is a baryon number density, and ε is a total energy density.

V [fm^3]	n_B [fm^{-3}]	ε [GeV/fm^3]
64.0	0.156	0.313 0.469 0.625 0.781 0.938 1.093
	0.234	0.469 0.625 0.781 0.938 1.093
	0.313	0.469 0.625 0.781 0.938 1.093
128.0	0.156	0.313 0.625 0.938
	0.234	0.469 0.781 1.093
	0.313	0.469 0.781 1.093
216.0	0.157	0.370 0.463 0.556 0.648 0.741 0.833
	0.231	0.370 0.463 0.556 0.648 0.741 0.833
	0.315	0.370 0.463 0.556 0.648 0.741 0.833

TABLE III. The relaxation time of number densities for each of particle species at $n_B = 0.156\text{fm}^{-3}$. These values are calculated from the exponential fit for fig.5.

ε [GeV/fm^3]	N (=Δ) [fm/c]	π [fm/c]	ρ [fm/c]
0.313	7.1 ± 0.4	9.2 ± 0.3	21.2 ± 0.7
0.625	9.8 ± 0.5	13.3 ± 0.3	44.9 ± 1.0
0.938	10.6 ± 0.6	18.6 ± 0.4	68.5 ± 1.3

TABLE IV. Parameters of fits for relations between pressures and energy densities.

n_B [fm^{-3}]	v_s^2	ε_0
0.157	0.2171 ± 0.0009	0.1163 ± 0.0026
0.231	0.2122 ± 0.0008	0.1633 ± 0.0023
0.315	0.2083 ± 0.0007	0.2188 ± 0.0021

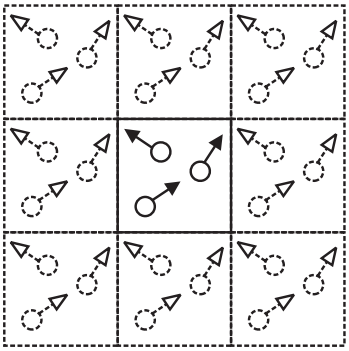

FIG. 1. This picture explains the idea of the periodic boundary condition. The box which is located in the center is a space of our interest. Here we call it the real box. We have to consider the collision between a particle in the real box and another particle in a replica.

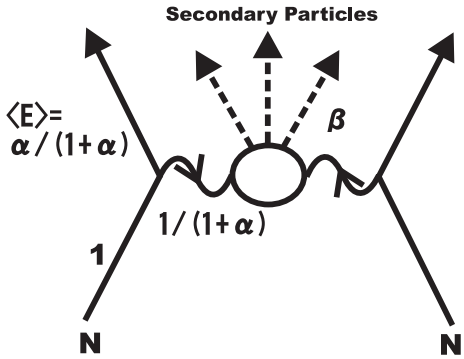

FIG. 2. The diagram of the multi-particle production process for the $N + N$ inelastic collision. Here $< E >$ denotes the average of the energy fraction which the leading nucleon carries after a collision. This quantity is related to the value of α which is one of adjustable parameters. The remainder of the energy fraction is consumed by the production of secondary particles whose momenta are determined according to the distribution which is given in eq.(11). Here β is the parameter of this distribution.

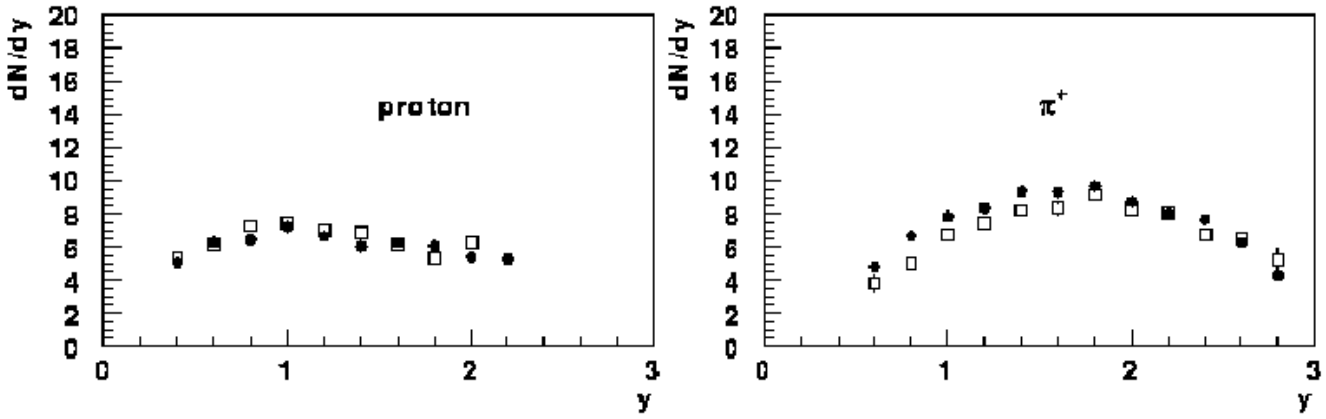

FIG. 3. A comparison between experimental results and our simulations. We study rapidity distributions of proton (left) and π (right) for S + Al central collisions at 14.6 GeV/nucleon, that are performed by E802 collaboration. Here squares denote results of our simulation, and filled circles are experimental results.

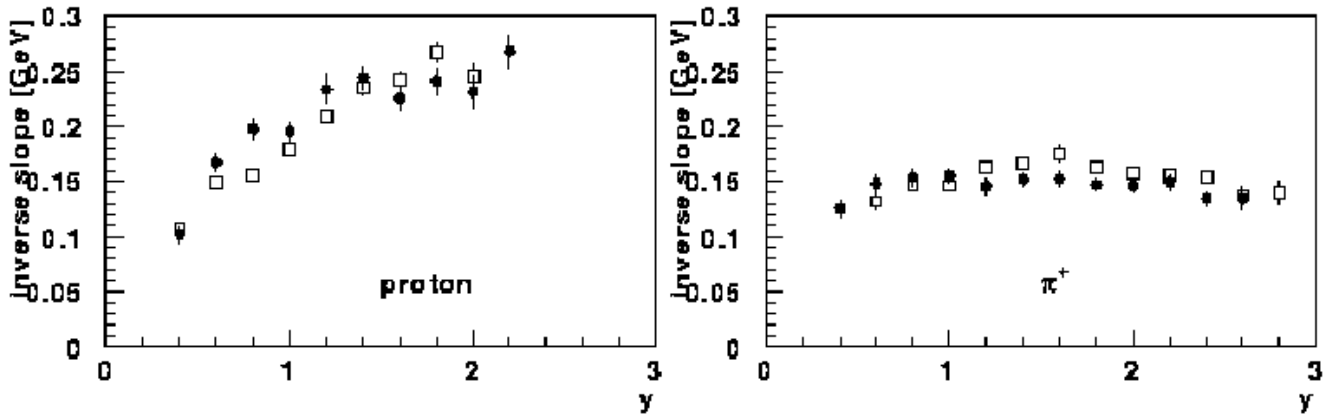

FIG. 4. A comparison between experimental results and our simulations. We study inverse slopes of transverse momentum distributions of proton (left) and π (right) for S + Al central collisions at 14.6 GeV/nucleon, that are performed by E802 collaboration. Here squares denote results of our simulation, and filled circles are experimental results.

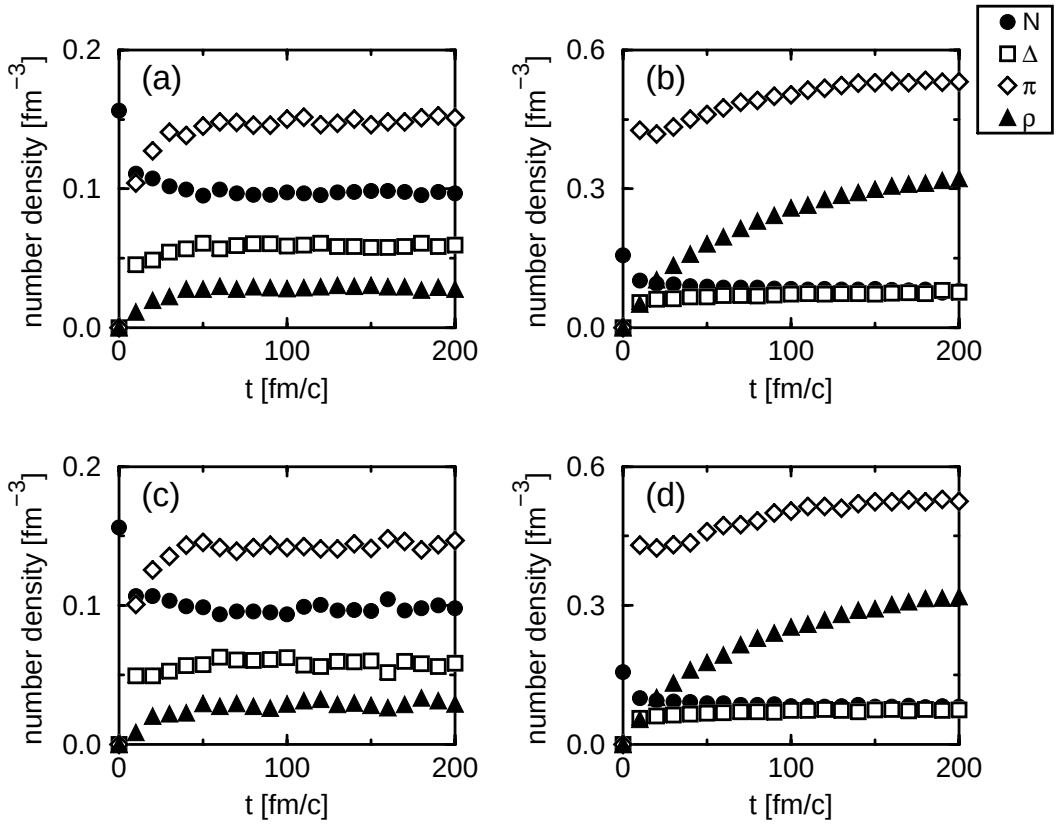

FIG. 5. The time evolution of number densities for each of particle species. Four different results are shown, (a). $V = 64.0\text{fm}^3$,$n_B = 0.156\text{fm}^{-3}$, $\varepsilon = 0.313\text{GeV/fm}^3$, (b). $V = 64.0\text{fm}^3$,$n_B = 0.156\text{fm}^{-3}$, $\varepsilon = 0.938\text{GeV/fm}^3$, (c). $V = 128.0\text{fm}^3$,$n_B = 0.156\text{fm}^{-3}$, $\varepsilon = 0.313\text{GeV/fm}^3$ and (d). $V = 128.0\text{fm}^3$,$n_B = 0.156\text{fm}^{-3}$, $\varepsilon = 0.938\text{GeV/fm}^3$.

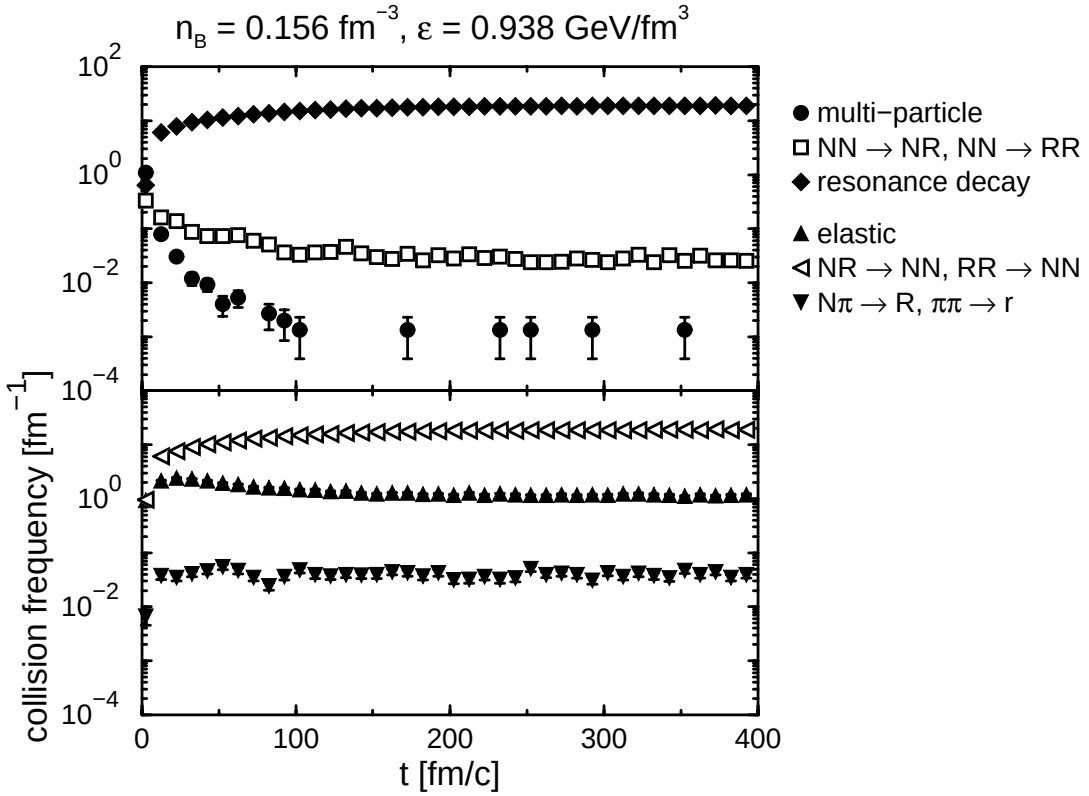

FIG. 6. The time evolution of collision frequencies for various types of collisions, i.e., 2-body collisions and decays that are already presented in eq.(3) $\sim$ (7), multi-particle productions and elastic collisions. Here R denotes baryon resonances, and r denotes meson resonances. The calculation is shown at $V = 64.0$ fm^3, $n_B = 0.156$ fm^{-3} and $\varepsilon = 0.938$ GeV/fm^3.

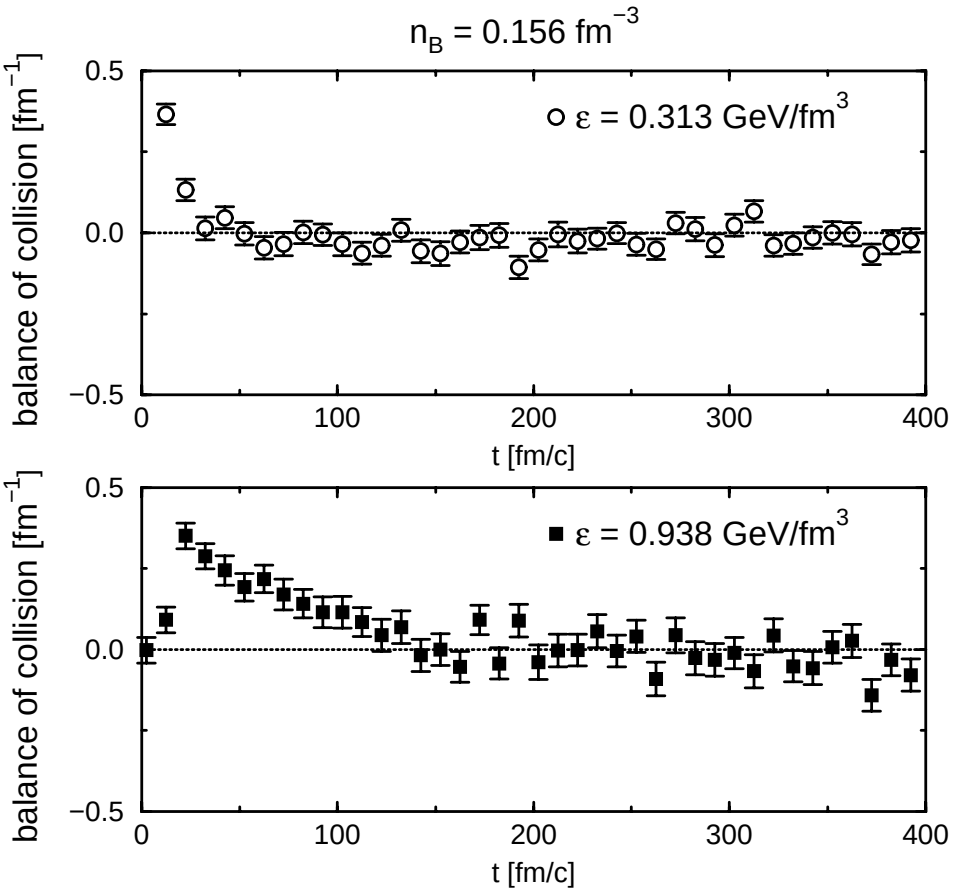

FIG. 7. The time evolution of the balance of collision frequencies at two different energy densities, $n_B = 0.156\text{fm}^{-3}$, $\varepsilon = 0.313\text{GeV/fm}^3$ and $n_B = 0.156\text{fm}^{-3}$, $\varepsilon = 0.938\text{GeV/fm}^3$. The quantity which corresponds to the vertical axis is defined as the difference between the collision frequency of production processes (eq.(3) $\sim$ (5)) and that of absorption processes (eq.(6), (7)). The system satisfies the detailed balance for $t \geq 150$ fm/c, therefore this quantity becomes zero when the equilibrium establishes.

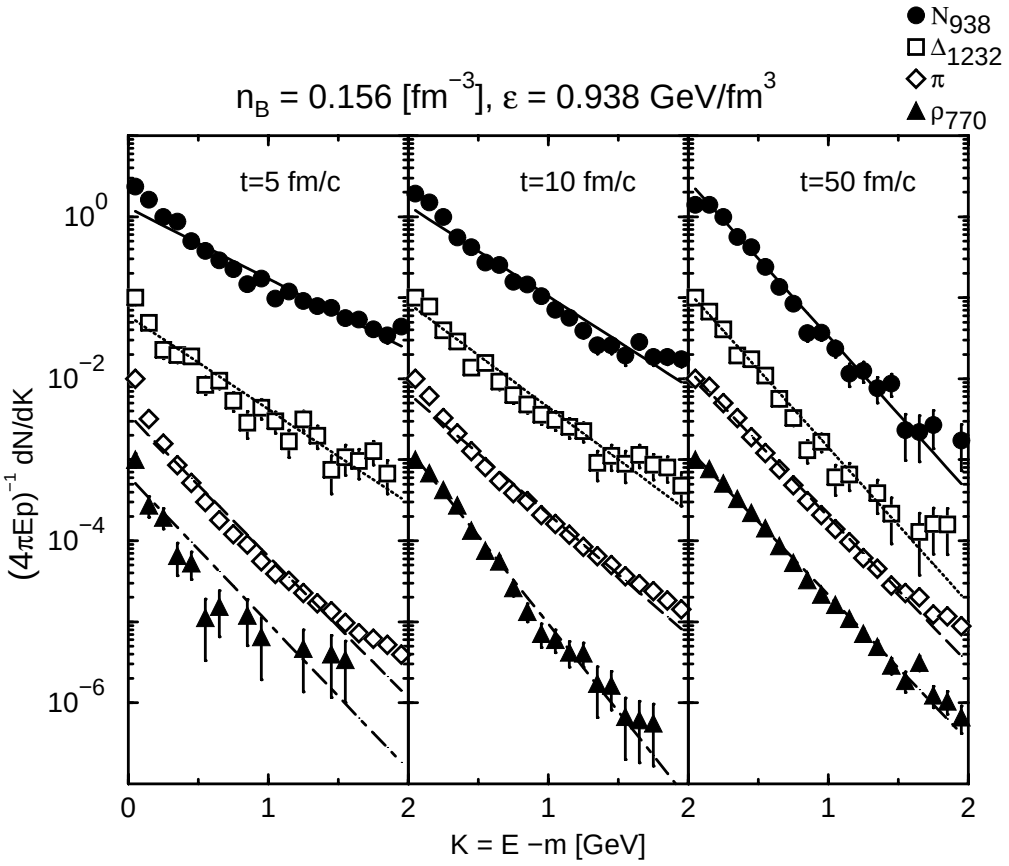

FIG. 8. Energy distributions of N_{938}, Δ_{1232}, π and ρ_{770} at three different values of time, i.e., $t = 5$ fm/c (left), $t = 10$ fm/c (center) and $t = 50$ fm/c (right). The lines are fitted results that are given by Boltzmann distributions.

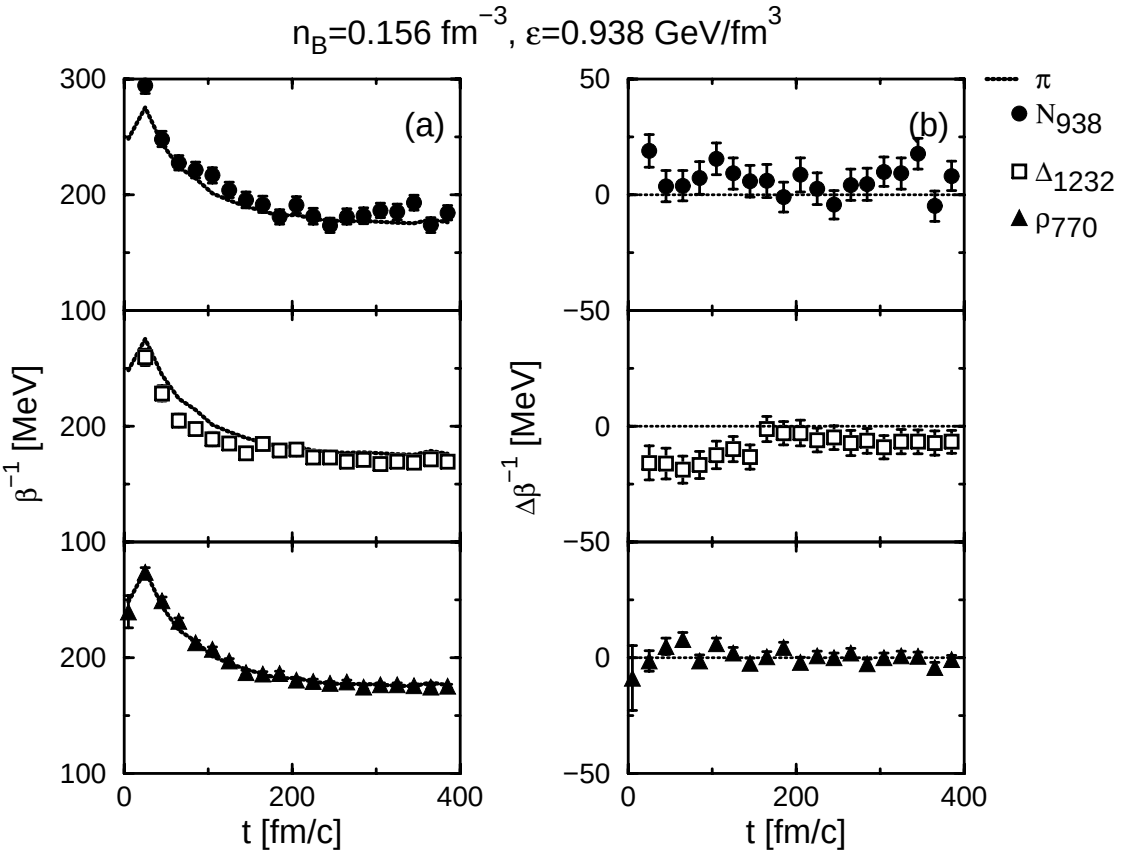

FIG. 9. (a). The time evolution of inverse slopes β^{-1} of N_{938}, Δ_{1232}, π and ρ_{770} at $n_B = 0.156$ fm^{-3}, $\varepsilon = 0.938$ GeV/fm^3. The value of β^{-1} is calculated from the fitting of energy distributions. Here the dotted line denotes the time evolution of β^{-1} for π. (b). The time evolution of $\Delta\beta^{-1}$ of N_{938}, Δ_{1232} and ρ_{770} at $n_B = 0.156$ fm^{-3}, $\varepsilon = 0.938$ GeV/fm^3. Here $\Delta\beta^{-1}$ is defined in eq.(14). The establishment of the thermal equilibrium can be confirmed by this figure.

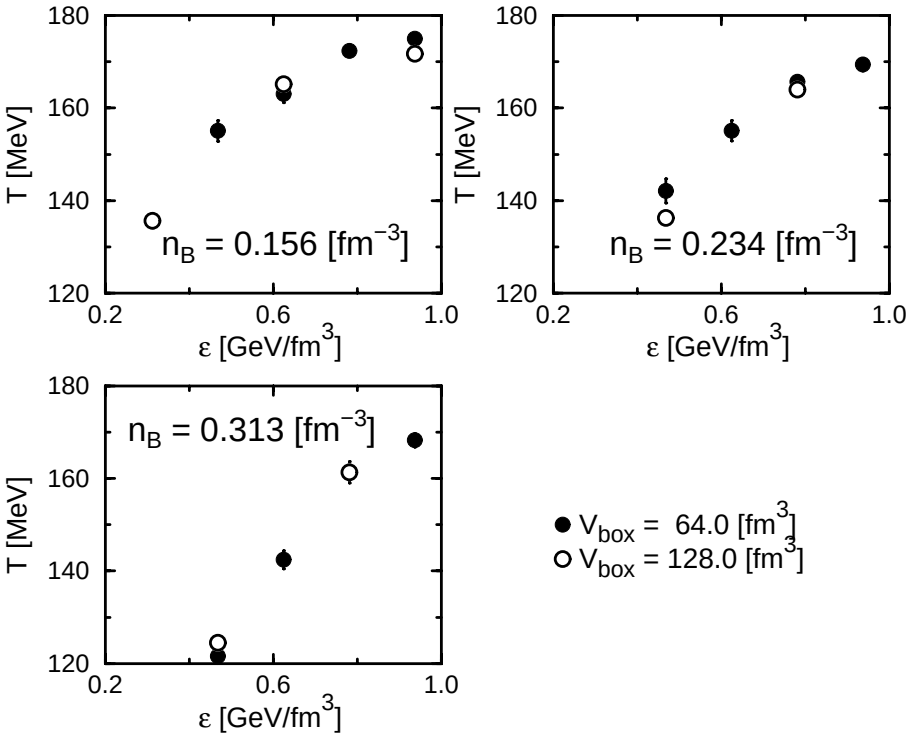

FIG. 10. The temperature of the system at various initial conditions. Results at $V = 64.0\text{fm}^3$ and $V = 128.0\text{fm}^3$ are compared.

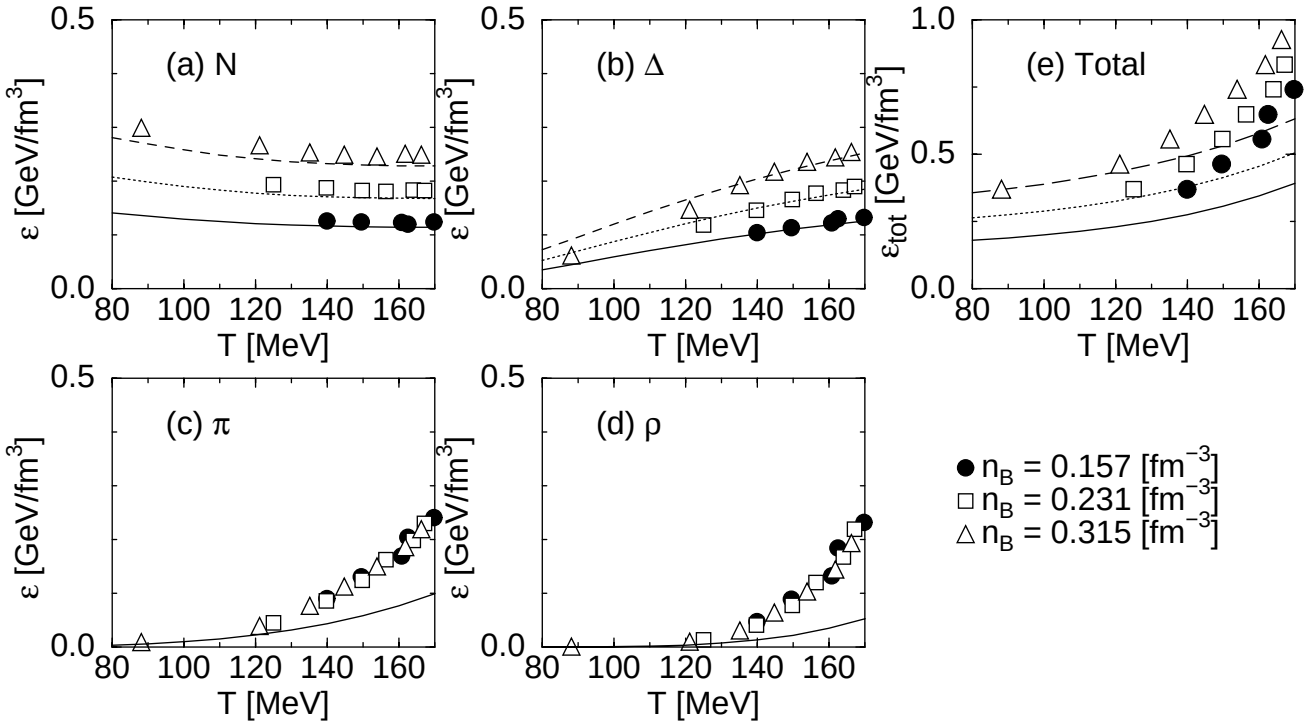

FIG. 11. The equation of state of the mixed hadron gas at the finite temperature ($80 < T < 170$MeV) and the finite baryon density ($0.157 < n_B < 0.315\text{fm}^{-3}$). Energy densities of (a) N, (b) Δ (the sum of all resonances), (c) π, (d) ρ_{770} and (e) total are plotted versus the temperature. The lines correspond to the results from the free gas model which is shown in Eq(17a).

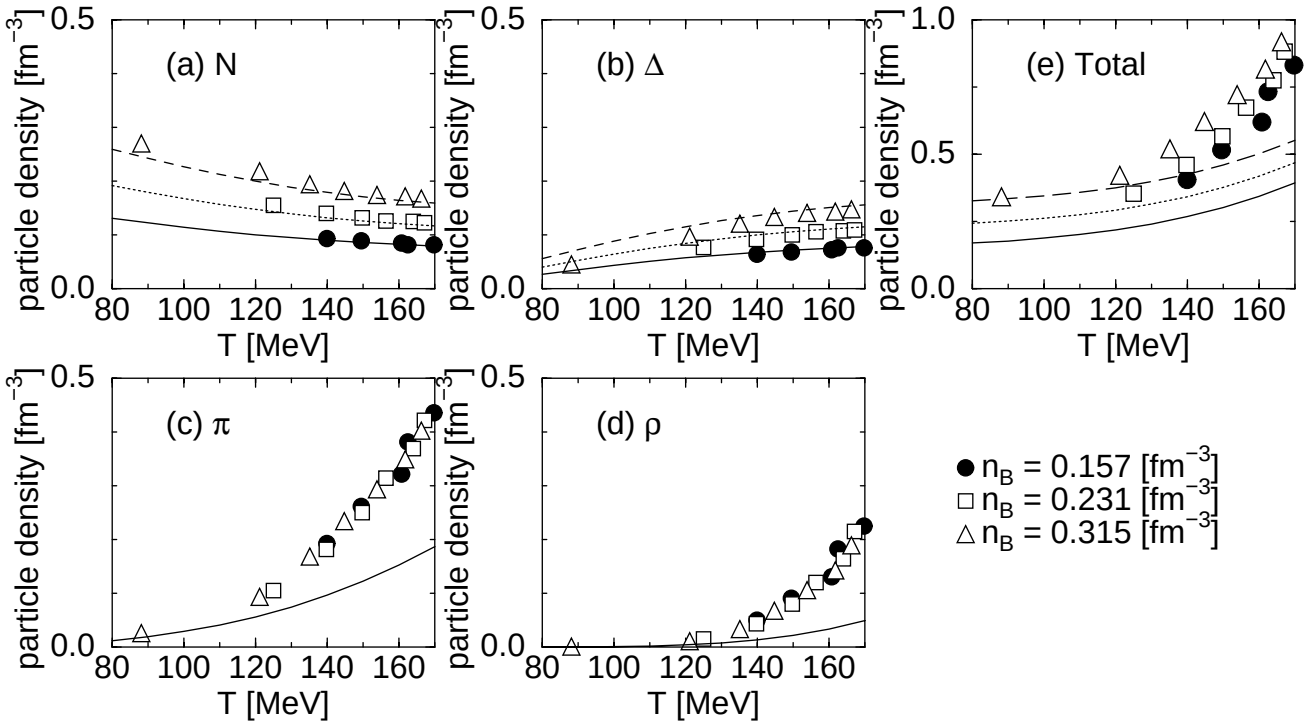

FIG. 12. Number densities of (a) N, (b) Δ (the sum of all resonances), (c) π, (d) ρ_{770} and (e) total are plotted versus the temperature. The lines correspond to the results from the free gas model which is shown in Eq(17b).

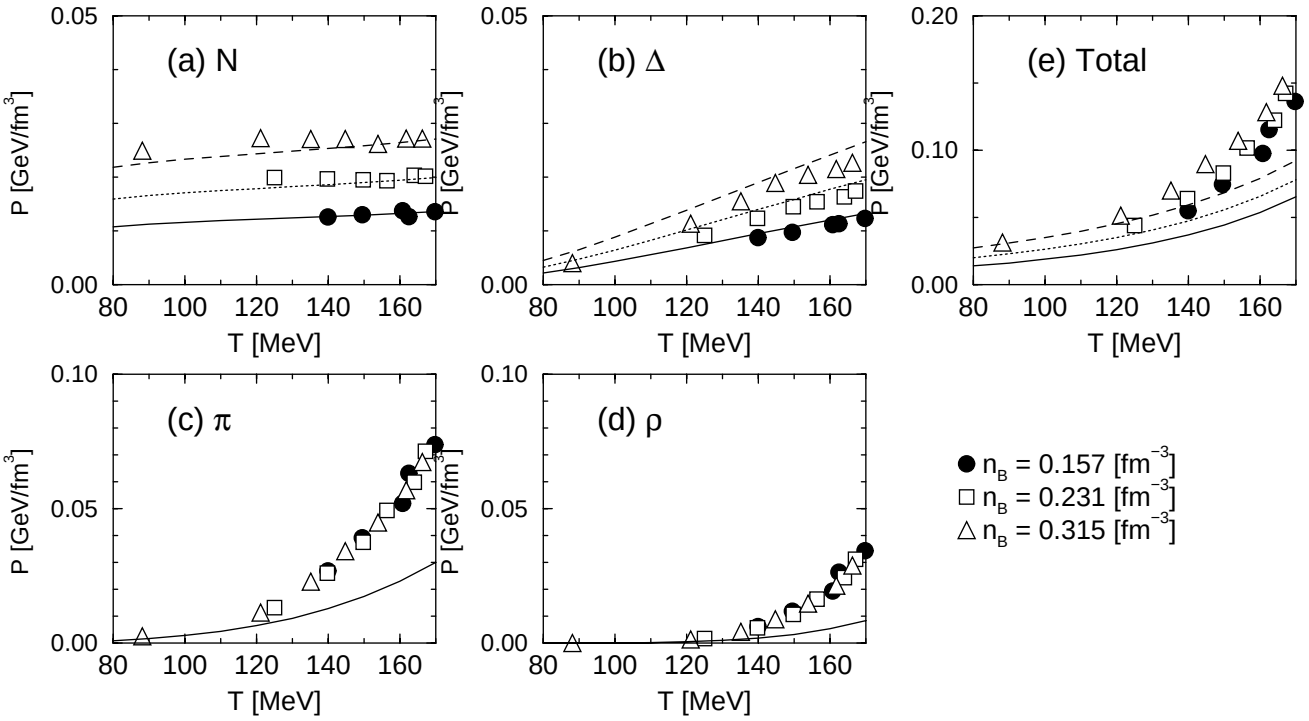

FIG. 13. Pressures of (a) N, (b) Δ (the sum of all resonances), (c) π, (d) ρ_{770} and (e) total are plotted versus the temperature. The lines correspond to the results from the free gas model which is shown in Eq(17c).

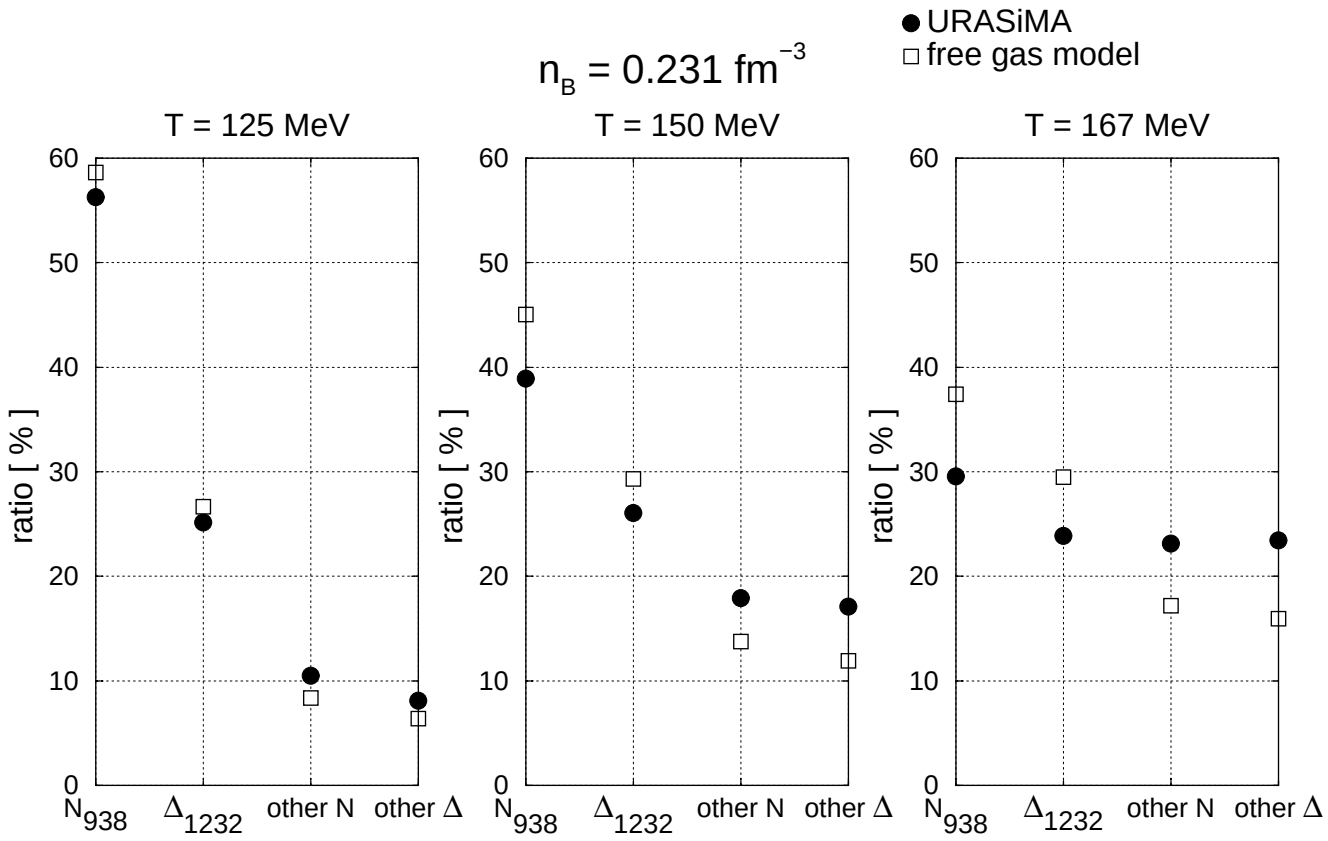

FIG. 14. The production ratio of N_{938}, Δ_{1232} and other heavy resonances N^*,Δ. Calculations are shown at $n_B = 0.231$ fm^{-3} and at the temperature $T = 125,\ 150,\ 167$ MeV.

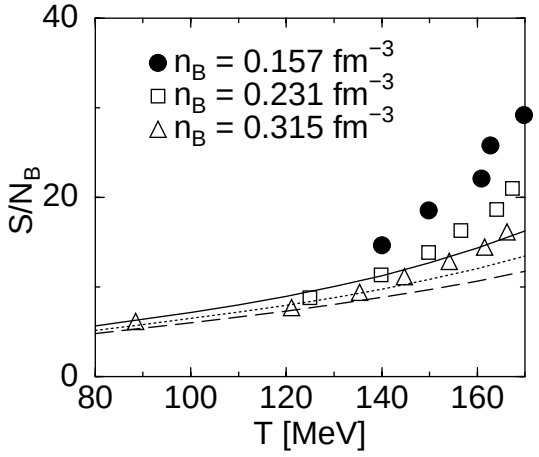

FIG. 15. The entropy per baryon is plotted versus the temperature. The definition of the entropy is given by eq.(18). The lines correspond to the results from the free gas model.

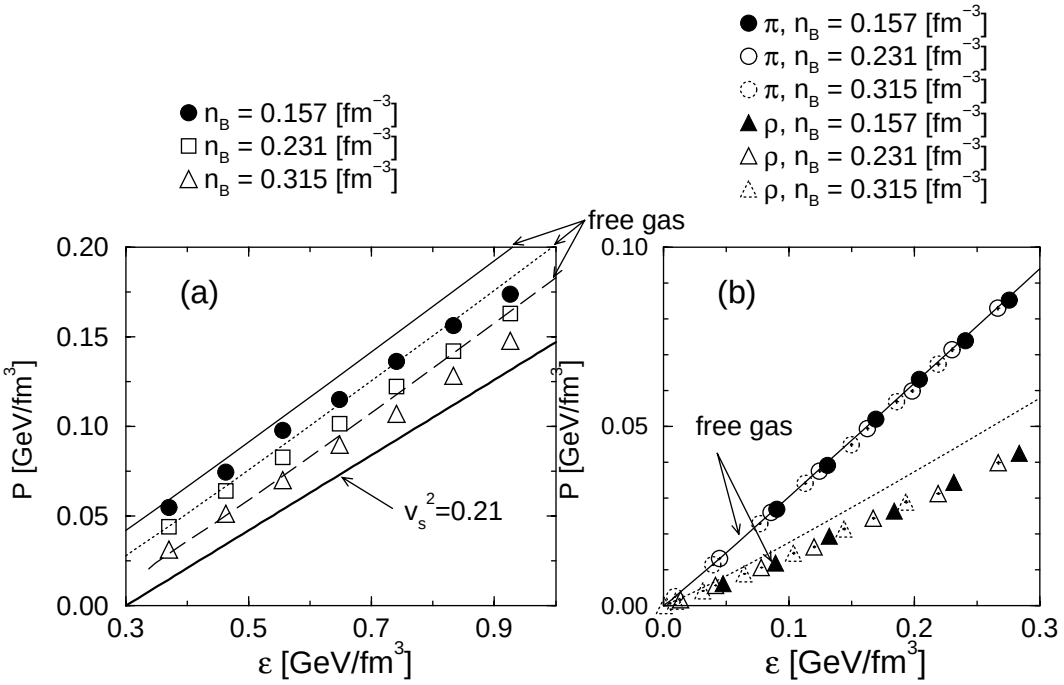

FIG. 16. (a). Pressures are plotted versus energy densities. Free gas results and the line whose slope is equal to 0.21 are also shown. (b). Partial pressures of mesons versus partial energy densities of them.

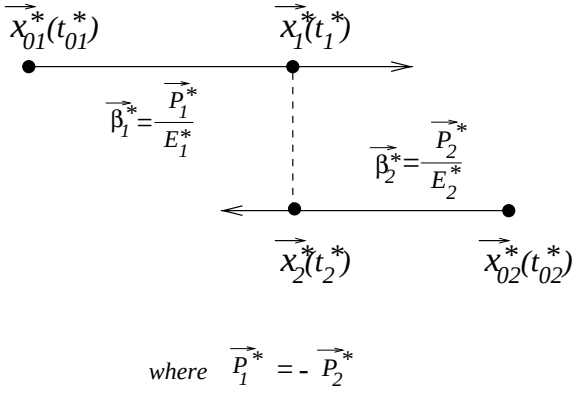

FIG. 17. The condition which the collision occurs in the CM frame of two particles. In this frame, the momentum vector of the particle p_1^*,p_2^* and the following vector $x_1^*(t_1^*) - x_2^*(t_2^*)$ cross each other at right angles when two particles get closest. In this situation, the collision occurs if eq.A3 is satisfied, and the impact parameter is defined as $b^* = |x_1^*(t_c^*) - x_2^*(t_c^*)|$, where t_c^* is the time collision occurs.